Microwave electromechanical resonator consisting of clamped carbon nanotubes in an abacus arrangement

H. B. Peng,* C. W. Chang, S. Aloni, T. D. Yuzvinsky, and A. Zettl†

Department of Physics and Center of Integrated Nanomechanical Systems, University of California at Berkeley
and Materials Sciences Division, Lawrence Berkeley National Laboratory, Berkeley, California 94720, USA

We describe nanoscale electromechanical resonators capable of operating in ambient-pressure air at room temperature with unprecedented fundamental resonance frequency of ~4 GHz. The devices are created from suspended carbon nanotubes loaded abacus style with inertial metal clamps, yielding short effective beam lengths. We examine the energy dissipation in the system due to air damping and contact loss. Such nanoabacus resonators open windows for immediate practical microwave frequency nanoelectromechanical system applications.

It has been said that the miniaturization of electronic devices has revolutionized the technology of today, while the miniaturization of mechanical devices will revolutionize the technology of the future. Nanoelectromechanical systems (NEMSs) with molecular-scale components operating at ultrahigh (microwave) frequencies promise applications ranging from single-atom mass and force sensing to efficient energy conversion systems to quantum computation. Despite recent nanotechnology advances facilitating the construction of very small scale devices, a seemingly insurmountable barrier has been the realization of practical (i.e., operating at room temperature in atmospheric pressure) ultrahigh frequency mechanical resonators. The challenge is twofold: materials must be fabricated with nanoscale dimension and with relatively defect-free surfaces, and detection methods with suitable sensitivity to the ultrasmall displacements must be employed.

We here report the construction and operation of nanotube-based "nanoabacus" devices functioning as self-detecting NEMS resonators, capable of operating in ambient-pressure air at room temperature with fundamental resonance frequency near 4 GHz. Specialized nonlinear mixing methods are used to detect the resonance. The devices are suitable for practical microwave frequency NEMS applications.[1,2]

Figure 1(a) shows schematically the resonator configuration. Single-wall carbon nanotubes (CNTs) are grown by chemical vapor deposition across a trench between metal source and drain electrodes on a silicon chip.[3–6] An independent gate electrode is located at the bottom of the trench. The device geometry and the typical device parameters are similar to those described in a previous work.[6] Following CNT growth, metal beads are placed abacus style on the CNTs by thermally evaporating metal (such as indium) over the entire device. Figure 1(b) shows a typical beaded or "mass loaded" CNT segment. When driven mechanically, the CNT exhibits transverse-beam-like flexure modes. The crucial point is that shortened CNT sections, between two adjacent indium beads, can serve as the resonating beam, and the short effective clamped length results in ultrahigh resonance frequencies. Placement of the beads is akin to a musician placing fingers on a musical string or wind instrument to select specific notes.

The device geometry of Fig. 1(a) lends itself well to electrostatic drive via applied voltages between the CNT and the gate electrode, and to nonlinear mixing methods for detection of the mechanical response. In previous work on nanotube-based resonators, both "1ω" mixing method[7] and "2ω" mixing method[6] have been used to probe the mechanical resonance of NEMS resonators. We here employ the high sensitivity 2ω mixing method to drive and electrically detect the mechanical motion of the nanoabacus resonator. A schematic circuit diagram of the drive and detection electronics for the 2ω method are shown in Fig. 2(a). With a sinusoidal actuation voltage signal applied to the gate at a frequency ω (forcing the CNT at 2ω, a natural consequence of the fact that the electrostatic force on a capacitor is proportional to the square of the voltage-induced charges), and a carrier sig-
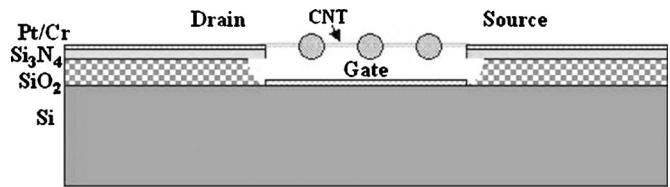
(a)
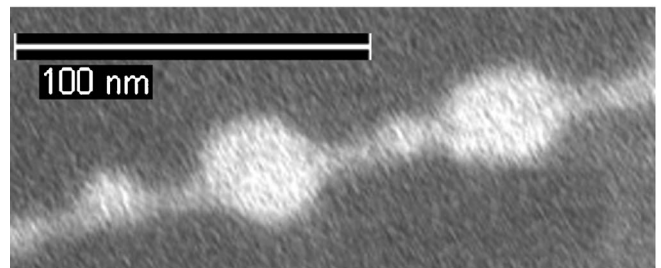
(b)

FIG. 1. Nanoabacus resonators. (a) Schematic cross section of the device. Suspended carbon nanotubes were grown bridging source and drain electrodes (Pt/Cr) (Refs. 3 and 4) with a local gate lying on the bottom of the trench (Ref. 5). An evaporation of materials such as indium on to the nanotube forms the abacus structure. (b) Scanning electron micrograph of a nanoabacus made by evaporating nominal 2.5 nm thick indium onto a CNT. Scale bar: 100 nm.
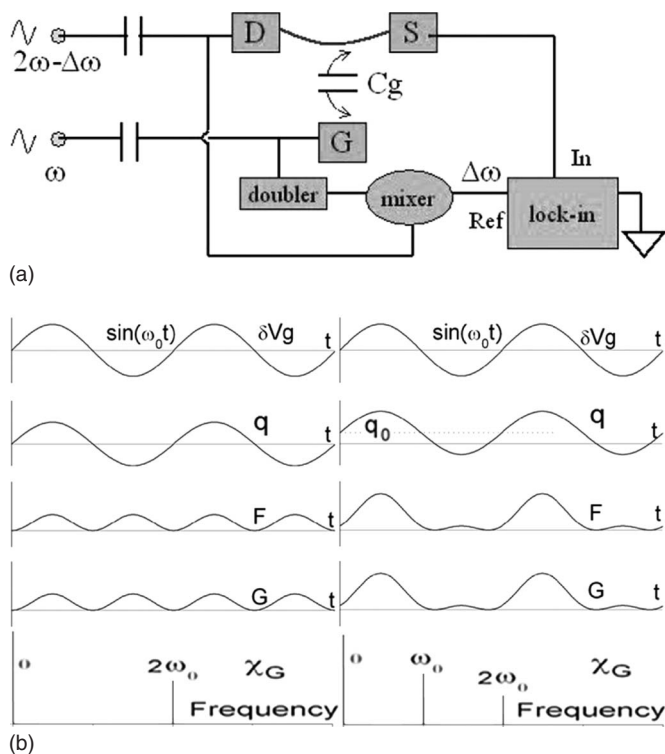
(a)

(b)

FIG. 2. (a) Schematic circuit diagram of the experimental setup for the 2ω mixing method. An actuation voltage signal of amplitude δV_g at a frequency ω is applied to the gate G, while a carrier voltage signal of amplitude δV_d is applied to the drain D at a frequency $2\omega-\Delta\omega$. The current flow through the source S at the frequency $\Delta\omega$ (typically set at 7 KHz) is monitored using a lock-in amplifier with a time constant of 300 ms. The lock-in reference at the frequency $\Delta\omega$ is obtained through a frequency doubler and a mixer. The effective driving frequency on the resonator is 2ω, the frequency of the electrostatic force induced by the gate voltage signal. (b) Illustration of actuation gate signal δV_g and the corresponding response in charge q, force F, conductance G, and Fourier transform of conductance χ_G under ideal conditions with no accumulated charge (left) and with finite accumulated charge q_0 (right).

nal applied to the drain at a frequency $2\omega-\Delta\omega$, the drain-source current is measured at the intermediate frequency $\Delta\omega$ (~7 kHz) by a lock-in amplifier. Using the nanotube as a nonlinear mixing element allows for "self-detection" of the mechanical motion without the need for more complex transduction (such as magnetomotive[8]). Note that the electrical conductance of a mechanically vibrating nanotube can be affected by the strain effect on the contacts, the strain effect along the nanotube, and the extra field effect due to the displacement-induced gate capacitance change. The experimentally observed significant conductance modulation suggests that the strain effect on the contacts possibly dominates the transduction[6] because the width of tunneling barriers strongly affects the electrical conductance (an exponential dependence).

Figure 2(b) illustrates how, with a gate signal frequency ω_0, the frequency spectrum of the nanotube conductance G displays a component at the doubled frequency $2\omega_0$. Here, q is the induced (capacitance) charge leading to an electrostatic force F on the CNT with q_0 the excess accumulated charge.

G is the resultant CNT electrical conductance, and χ_G is the Fourier transform of G. To estimate the capacitance between the CNT and the gate electrode, we neglect the contribution of the density of states in the nanotube and treat the device as a pure electrostatic system with a long equipotential cylinder (the nanotube) above a semi-infinite equipotential plate (the gate). Using the image-charge method, we can transform the problem into the standard case with two long parallel cylinders and obtain the capacitance of the system as

$$C_g = \frac{2\pi\varepsilon_0 L}{\ln[(W/r) + \sqrt{(W/r)^2 - 1}]},$$

where L is the nanotube length, r is the nanotube radius, and W is the distance between the gate electrode and the center of the nanotube. The electrostatic force per unit length on the CNT can be expressed as

$$F = \frac{1}{8\varepsilon_0 W L^2}\left[q_0^2 + \frac{(C_g\delta V_g)^2}{2} + 2q_0 C_g\delta V_g \cos(\omega t) \right.$$
$$\left. + \frac{(C_g\delta V_g)^2}{2}\cos(2\omega t) \right],$$

where δV_g is the amplitude of the gate electrical signal and the excess charge q_0 is assumed to have sufficient mobility to be tuned by a rf gate signal. We further assume a linear response of the nanotube electrical conductance to the position displacement.

The left column presents the ideal case where there is no accumulated static charge ($q_0=0$) near the CNT. Under such "ideal" conditions, the conductance response only displays a 2ω component in the Fourier spectrum, i.e., the effective actuation frequency is 2ω, instead of the gate voltage frequency ω. In this special case, an experiment performed using the 2ω method would show a strong resonance, while a measurement using the 1ω method would yield no resonance signal at all. The right column in Fig. 2(b) shows the more general case with finite accumulated charge q_0 influencing the nanotube. In this case, both 1ω and 2ω components appear in the conductance response. As the accumulated charge q_0 increases, the 1ω component increases and eventually dominates the response (assuming q_0 has sufficient mobility to be modulated by the rf gate signal). However, for certain nanoscale devices excess static charges can be strongly trapped in defect states and have low mobility.[6,9] In this case, the relative strength of the 1ω and 2ω components does not depend on the excess charge q_0. Hence, the mechanical response at ω_0 and $2\omega_0$ reflects the excess device charge and the mobility thereof.[6]

Figure 3 gives the room-temperature electrical response of a nanoabacus resonator. A fundamental mode resonance[10–12] is clearly observed at 3.80 GHz at a pressure of 10^{-6} Torr (triangles) and at 3.79 GHz at atmospheric pressure (circles). The pressure-induced shift is likely due to the adsorption of air-specific molecules (such as water or oxygen) on the CNT, leading to a change of the resonator mass. Such extreme molecular-level mass sensitivity is an intrinsic advantage of light-mass NEMS resonators. We note that for suspended bare CNT resonators, the mechanical resonance is
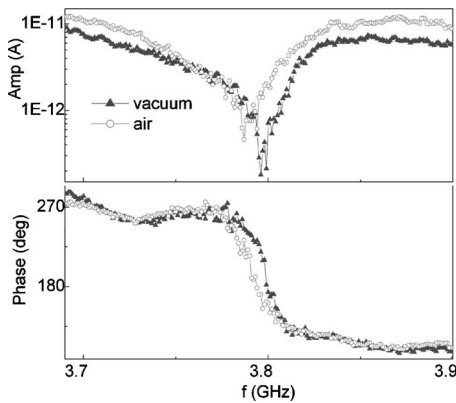
FIG. 3. Amplitude (in logarithmic scale) and phase of the electrical current as a function of effective driving frequency f in a vacuum of 10^{-6} Torr (triangles) and in air (circles) for a nanoabacus resonator, measured with a gate signal $\delta V_g = 158$ mV and a drain signal $\delta V_d = 70$ mV by the 2ω mixing method. The resonator was made by coating a suspended carbon nanotube device with thermally evaporated 5 nm thick indium (measured by a quartz crystal monitor). The trench between the source and the drain electrodes is 300 nm wide and 400 nm deep. A metal gate (Pt 20 nm/Cr 5 nm) was patterned on the bottom of the trench. The nanotube was grown by chemical vapor deposition (Ref. [6]) directly bridging the source and the drain electrodes (Pt 20 nm/Cr 5 nm) with electrical contact, and the electrical resistance is ~ 1 MΩ. We also observed other lower-frequency resonance at 0.27, 0.45, and 1.2 GHz, likely induced by different resonating beam sections.

usually much weaker in atmospheric pressure, or even not detectable at all.[7] However, as shown in Fig. 3, microwave operation in air can be easily achieved with nanoabacus resonators.

From the full width at half depth from the amplitude data, we estimate that the quality factor Q changes from ~ 58 in a vacuum of 10^{-6} Torr to ~ 44 in ambient-pressure air. Note that the phase signal (Fig. 3) experiences a much sharper change at the resonance, which has been explained[6] as a result of the interference effect of the background response and the resonance response. On resonance in vacuum, within a frequency range of 9 MHz, there is an easily detectable phase change of $\sim 72°$ (half of the total phase change due to the resonance). In analog to a pure Lorentzian-type signal, we define a "phase quality factor" $Q_p = \omega_0/\Delta\omega_1$, where ω_0 is the resonance frequency and $\Delta\omega_1$ is the frequency interval by which the phase change accounts for 50% of the total phase change near resonance. Here, we have $\Delta\omega_1 \sim 9$ MHz, leading to an effective phase quality factor $Q_p \sim 420$. Therefore, the phase signal offers great advantage in detecting the frequency shift for sensing applications.

The fundamental mode resonance frequency ω_0 is related to resonator physical properties by

$$\omega_0/2\pi = 1.259\sqrt{E/\rho}(d/L^2), \qquad (1)$$

where E is Young's modulus, ρ is the density, d is the diameter, and L is the length of the doubly clamped CNT. To obtain Eq. (1), the CNT is treated as a thin-wall cylinder. With $d = 3.5$ nm, $\rho = 2.25$ g/cm^3 (density of graphite), and
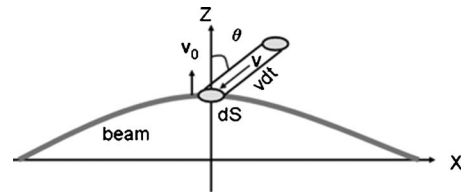

FIG. 4. Schematic diagram of a collision between a gas molecule with velocity $V(v, \theta, \phi)$ and a vibrating beam with velocity V_0 along the z axis.

$\omega_0/2\pi = 3.8$ GHz relevant for the device of Fig. 3, and taking $E \sim 100$ Gpa,[13] we estimate an effective vibrating beam length $L \sim 90$ nm, consistent with longer CNT sections between inertial clamps as observed by scanning electron microscope. In light of the $1/L^2$ scaling of the resonance frequency, the beaded CNT approach offers great potential in realizing NEMS resonators with extremely high resonance frequency even into the terahertz region. Indeed, the shorter CNT segments depicted in Fig. 1(b) of typical length of ~ 10 nm are expected to resonate at ~ 0.4 THz.[14] In principle, the bead positions (and hence resonance frequencies) are tunable postproduction, using a current-induced mass conveyor mechanism.[15]

To our knowledge, the resonator with nanoabacus configuration is the first reported air-operational practical NEMS resonator in the several gigahertz range. To gain insight into the mechanism of ambient-pressure operation, we address below the issue of energy dissipation and analyze the quality factor Q of the system. For a doubly clamped beam resonator, the energy dissipation can occur either through the air in contact with the beam (air damping) or through the supports in contact with the substrate (contact dissipation). One example of the contact dissipation is the anchor loss, with macroscopic mechanical waves radiating through the contacts into the substrate. Due to the coupling between the resonator motion and the microscopic phonon modes, phonon-phonon scattering, and electron-phonon scattering, the contact dissipation can also occur through phonon transport or electron transport at the contacts. There have been many interests in quantitative analyses of NEMS loss mechanisms.[16–22] Here, we explore the issue theoretically and compare the results with the experimental values obtained in our devices.

Air damping can occur in the molecular region or the viscous region, depending on the ratio of the mean free path of gas molecules to the size of the resonator beam.[18–20] The molecular mean free path l_{mfp} can be expressed[18,23] as $l_{mfp} = 0.23kT/D^2p$, where k is the Boltzmann constant, D the diameter of gas molecules, T the temperature, and p the pressure. For air at standard condition,[18] l_{mfp} is ~ 65 nm. The typical diameter d of single-wall carbon nanotube resonators is $1-5$ nm. Therefore, $l_{mfp}/d > 10$, and the air damping should be in the molecular region, i.e., the damping is mainly caused by the momentum transfer due to collisions between air molecules and the moving surface of the vibrating beam. Here, we use the kinetic theory of gases to estimate the drag force (Fig. 4). Since the air molecule mass m is much less than the resonator mass M, a collision from a molecule moving opposite to the vibrating resonator beam induces a momentum loss of $2m(V_z + V_0)$ to the beam in the elastic scat-

tering limit, where V_z is the velocity of the molecule and V_0 is the velocity of the beam. On the other hand, a collision with the molecule moving in the same direction as the beam contributes a momentum gain of $2m(V_z - V_0)$ to the resonator beam. As illustrated in Fig. 4, for molecules with a velocity $V(v, \theta, \phi)$ (in spherical coordinates), within a small time interval dt only those inside the cylinder can collide with the beam surface dS. Summing up the contributions of collisions from both sides of the beam, we obtain, using a Maxwellian distribution, a net momentum transfer,

$$\Delta P = \int_0^\infty \left(\frac{m}{2\pi kT} \right)^{3/2} e^{-mv^2/2kT} v^2 dv \int_0^{\pi/2} \sin\theta d\theta$$

$$\times \int_0^{2\pi} d\phi n dS v dt \sin\theta 4mV_0$$

$$= \sqrt{2\pi mkT} n V_0 dS dt, \qquad (2)$$

where n is number of molecules per unit volume. The resultant net drag force per unit area is

$$\Delta F = \sqrt{2\pi mkT} n V_0 = \sqrt{\frac{2\pi m}{kT}} p V_0, \qquad (3)$$

where we have used $n = p/kT$ for the ideal gas, with p the air pressure. This leads to a damping term in the Euler-Bernoulli equation as

$$\rho A \frac{\partial^2 u(x,t)}{\partial t^2} + EI \frac{\partial^4 u(x,t)}{\partial x^4} + \eta \frac{\partial u(x,t)}{\partial t} = f(x) e^{-i\omega t}, \qquad (4)$$

where $u(x,t)$ is the displacement of beam neutral axis, ρ is the beam density, A is the beam cross-sectional area, E is Young's modulus, I is the bending moment of inertia, $f(x)$ is the drive force per unit length, and ω is the drive frequency. From Eq. (3), the damping coefficient η is obtained as

$$\eta = \sqrt{\frac{2\pi m}{kT}} p b, \qquad (5)$$

with b being the beamwidth.

Solving the Euler-Bernoulli equation gives a fundamental mode amplitude,

$$a_0 = \frac{c}{\omega_0^2 - \omega^2 - i \dfrac{\omega_0 \omega}{Q_{air}}}, \qquad (6)$$

with c a constant (independent of ω) and ω_0 the fundamental mode resonance frequency. The air-damping-induced quality factor is

$$Q_{air} = \omega_0 \frac{\rho A}{\eta}. \qquad (7)$$

From Eqs. (5) and (7), we obtain theoretically an air-damping quality factor $Q_{air} \sim 143$ in the elastic scattering limit for the device shown in Fig. 3 by taking a beamwidth $b = 3.5$ nm, a beam cross-sectional area $A = 8$ nm^2, a density $\rho = 2.25$ g/cm^3, and a resonance frequency $\omega_0/2\pi = 3.8$ GHz.

Considering the contribution from both the air damping and the contact dissipation, the overall quality factor Q satisfies $1/Q = 1/Q_{air} + 1/Q_{contact}$, where Q_{air} and $Q_{contact}$ are induced by the air and the contacts, respectively. In a vacuum of 10^{-6} Torr, the contribution due to air damping is negligible and the contact dissipation dominates the Q factor. Therefore, for the device shown in Fig. 3, we can estimate a contact-induced quality factor from the experimentally observed total quality factor, $Q_{contact} \sim 58$. From the data in air, the overall Q decreases to ~ 44. Thus, we can extract an air-induced quality factor from the experiment as $Q_{air} = (1/Q - 1/Q_{contact})^{-1} \sim 182$, which is close to the theoretical value of ~ 143 estimated above.

An important point from Eq. (7) is that the air-induced quality factor is proportional to the resonance frequency. Thus, a higher quality factor can be obtained with a higher resonance frequency and this naturally explains why room-temperature air operation is realized in our microwave frequency nanoabacus resonator, while operation above a pressure of 10 Torr is not possible in resonators with a lower frequency.[7]

The abacuslike beaded CNT approach provides a unique way to easily fabricate suspended NEMS devices beyond the reach of current lithographic technology. The devices can be integrated into higher-order NEMS structures, and therefore pave the way for future practical applications.

*haibingpeng@post.harvard.edu

†azettl@berkeley.edu

[1] R. G. Knobel and A. N. Cleland, Nature (London) **424**, 291 (2003).

[2] J. C. Meyer, M. Paillet, and S. Roth, Science **309**, 1539 (2005).

[3] H. B. Peng, T. G. Ristroph, G. M. Schurmann, G. M. King, J. Yoon, V. Narayanamurti, and J. A. Golovchenko, Appl. Phys. Lett. **83**, 4238 (2003).

[4] H. B. Peng and J. A. Golovchenko, Appl. Phys. Lett. **84**, 5428 (2004).

[5] J. Cao, Q. Wang, D. Wang, and H. Dai, Small **1**, 138 (2005).

[6] H. B. Peng, C. W. Chang, S. Aloni, T. D. Yuzvinsky, and A. Zettl, Phys. Rev. Lett. **97**, 087203 (2006).

[7] V. Sazonova, Y. Yaish, H. Ustunel, D. Roundy, T. A. Arias, and P. L. McEuen, Nature (London) **431**, 284 (2004).

[8] X. M. H. Huang, C. A. Zorman, M. Mehregany, and M. L.

Roukes, Nature (London) **421**, 496 (2003).

[9] H. B. Peng, M. E. Hughes, and J. A. Golovchenko, Appl. Phys. Lett. **89**, 243502 (2006).

[10] Under appropriate driving conditions, higher mode resonance can also be excited (see, for example, Refs. 11 and 12). In our device geometry with a single gate as the electrostatic driving source, the fundamental mode resonance should dominate, because the decomposition components of such a driving force profile into higher-mode eigenfunctions (with more than one nodes) should be small. The lower resonance frequencies observed in the specific sample relevant to Fig. 3 (as listed in the caption) do not have a difference-mode eigenfrequency relationship, and are most likely induced by different resonating beam sections.

[11] I. Bargatin, I. Kozinsky, and M. L. Roukes, Appl. Phys. Lett. **90**, 093116 (2007).

[12] S. Dohn, R. Sandberg, W. Svendsen, and A. Boisen, Appl. Phys. Lett. **86**, 233501 (2005).

[13] *Carbon Nanotubes: Synthesis, Structure, Properties, and Applications*, edited by M. S. Dresselhaus, G. Dresselhaus, and P. Avouris (Springer, Berlin, 2001).

[14] The detection of such extremely high frequency resonance is limited by our current experimental instrumentations, such as the signal source and external circuit components operational in terahertz frequency range.

[15] B. C. Regan, S. Aloni, R. O. Ritchie, U. Dahmen, and A. Zettl, Nature (London) **428**, 924 (2004).

[16] M. R. Geller and J. B. Varley, e-print arXiv:cond-mat/0512710.

[17] R. Lifshitz and M. L. Roukes, Phys. Rev. B **61**, 5600 (2000).

[18] R. B. Bhiladvala and Z. J. Wang, Phys. Rev. E **69**, 036307 (2004).

[19] F. R. Blom, S. Bouwstra, M. Elwenspoek, and J. H. J. Fluitman, J. Vac. Sci. Technol. B **10**, 19 (1992).

[20] K. Yum, Z. Wang, A. P. Suryavanshi, and M. Yu, J. Appl. Phys. **96**, 3933 (2004).

[21] D. M. Photiadis and J. A. Judge, Appl. Phys. Lett. **85**, 482 (2004).

[22] M. C. Cross and R. Lifshitz, Phys. Rev. B **64**, 085324 (2001).

[23] F. Reif, *Fundamentals of Statistical and Thermal Physics* (McGraw Hill, New York, 1965).